Modeling, Analysis, and Experimental Validation of Inverter Fault Response under Grid Disturbances

Rasel Mahmud
New York Power Authority
Albany, New York, USA
rasel.mahmud@nypa.gov

James Cale
Colorado State University
Fort Collins, Colorado, USA
james.cale@colostate.edu

***Abstract*—This study presents a detailed mathematical framework for analyzing the behavior of inverter-based resources (IBRs) under grid disturbances using the dq-reference frame. The dynamics of dq-currents are modeled, considering nonlinearities introduced by controller saturation and current limiting. Theoretical solutions for the transient and steady-state response of the dq-currents are derived, capturing the impact of coupling between active and reactive components. We investigate the effect of PWM saturation and the role of phase-locked loop (PLL) errors in disrupting the dq-transformation. Additionally, experimental validation with a commercial-off-the-shelf inverter subjected to an unbalanced fault confirms the theoretical findings. Key observations include the presence of transient oscillations, active-reactive coupling, prolonged settling times, and current limiting.**

***Index Terms*—Inverter-based resources (IBRs), fault ride-through (FRT), short-circuit response.**

I. Introduction

As power systems shift from synchronous-machine–dominated networks to converter-based grids, the nature of short-circuit behavior is fundamentally changing. Inverter-Based Resources (IBRs)—including PV inverters, modern wind turbines, and battery storage—do not produce fault currents governed by subtransient reactance, but instead by software-enforced limits, PLL behavior, and fast electronic controls operating in the dq frame [1]. As a result, IBR fault responses differ widely across technologies and challenge assumptions embedded in traditional protection and stability methods.

Grid codes increasingly attempt to standardize this behavior. IEEE 1547 specifies low-voltage ride-through requirements for distribution-connected IBRs, while IEEE 2800 extends these requirements to bulk power system IBR plants with explicit voltage–time ride-through envelopes, dynamic voltage support obligations, and mandatory negative-sequence current capability [2], [3]. European NC RfG and the GB Grid Code similarly mandate positive-sequence support and define options for negative-sequence injection and fast fault current injection (FFCI) [4], [5]. However, these documents specify only minimum performance—not the underlying dynamic behavior.

In practice, nested inverter control loops (PLL, dq current control, PWM, and internal protection) may saturate or become nonlinear during faults. Combined with current limiting and PLL angle/frequency errors, these effects distort the abc–dq transformation, couple active and reactive channels, and can induce oscillatory or even limit-cycle dq-current dynamics.

Accurate modeling of these effects is critical for protection studies, reduced-order model development, EMT simulations, and grid-code compliance validation [6]. Existing studies often address individual components—e.g., the impact of PLL dynamics on stability or the limitations of PI controllers during reactive current injection—but a unified, mathematically rigorous treatment of the fault-time dynamics in the dq frame remains limited. In particular, few works provide closed-form expressions for saturated dq-current trajectories or quantify the oscillatory behavior introduced by nonlinear current limiting, despite their importance to short-circuit and protection analysis.

This paper addresses this gap by providing a unified analytical and experimental study of dq-current dynamics in grid-following IBRs under unbalanced and faulted conditions. The main contributions are:

- Analytical treatment of controller saturation, PWM voltage limits, and current limiting, yielding closed-form expressions for saturated dq-current trajectories.
- Quantification of PLL angle and frequency error effects, showing their influence on dq-component distortion and oscillatory behavior.
- Identification of nonlinear conditions that lead to oscillations and limit cycles through linearized and nonlinear analyses.

II. DQ-Current Dynamics

Grid-tied inverters are commonly controlled in the synchronously rotating dq-reference frame, where three-phase voltages and currents are transformed into a rotating coordinate system aligned with the grid voltage angle $\theta(t)$ obtained from the phase-locked loop (PLL), as illustrated in Fig. 1. Starting from the inverter-side voltage equation of an L-filter in the stationary frame,

$$\mathbf{v}_{abc}(t) - \mathbf{v}_{\mathrm{g},abc}(t) = R_f \mathbf{i}_{abc}(t) + L_f \frac{d\mathbf{i}_{abc}(t)}{dt}, \qquad (1)$$

and applying the Park transformation into the synchronously rotating frame aligned with $\theta(t)$, the current dynamics can be

979-8-3315-8138-1

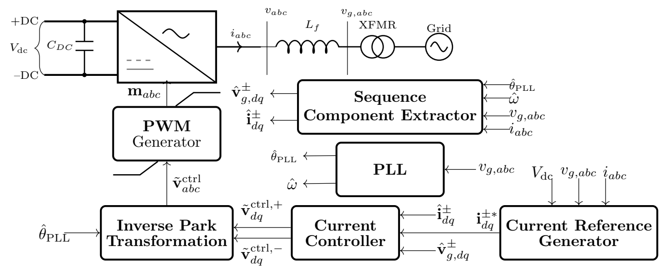

Fig. 1. Control architecture for a grid-tied inverter.

expressed in the *dq*-frame. If the PLL synchronizes the rotating reference frame such that the *d*-axis is aligned with the grid voltage vector, the quadrature-axis grid voltage component becomes zero, i.e., $v_{\mathrm{g},q}(t) = 0$. Under this commonly adopted assumption, the resulting *dq*-axis current dynamics for an inverter with an L-filter are given by:

$$\frac{di_d(t)}{dt} = -\frac{R_f}{L_f} i_d(t) + \omega i_q(t) + \frac{v_d(t) - v_{\mathrm{g},d}(t)}{L_f}, \quad (2)$$

$$\frac{di_q(t)}{dt} = -\frac{R_f}{L_f} i_q(t) - \omega i_d(t) + \frac{v_q(t)}{L_f}. \quad (3)$$

Here, $i_d(t)$ and $i_q(t)$ denote the inverter output currents in the synchronous reference frame, $v_d(t)$ and $v_q(t)$ are the inverter terminal voltages generated by the modulation stage, and $v_{\mathrm{g},d}(t)$ represents the grid voltage at the point of common coupling (PCC). The parameters R_f and L_f correspond to the resistance and inductance of the output filter shown in Fig. 1. The cross-coupling terms $\pm\omega i_{q,d}$ arise due to the rotating reference frame and are typically compensated in the inner current control loop.

III. Saturation and Current Limiting

During grid disturbances, such as faults, inverters encounter non-linear behavior due to *controller saturation* and *current limiting*. This section provides a mathematical treatment of saturation and current limiting mechanisms, and their effects on dq-currents.

A. Mathematical Model of Saturation

Inverter controllers operate within finite limits, and *saturation* occurs when the control output exceeds these bounds. The saturation nonlinearity is modeled as:

$$u_{\mathrm{sat}}(t) = \begin{cases} u_{\max} & \text{if } u(t) > u_{\max}, \\ u_{\min} & \text{if } u(t) < u_{\min}, \\ u(t) & \text{otherwise,} \end{cases} \quad (4)$$

where $u(t)$ is the unsaturated control signal and $u_{\max}$ and $u_{\min}$ denote the upper and lower limits, respectively.

During grid faults, saturation primarily arises from two mechanisms. *Controller saturation* occurs when the control command exceeds the inverter's modulation capability, causing integrator windup in PI controllers and resulting in delayed current tracking and prolonged transient recovery. *PWM saturation* occurs when the modulation index reaches its maximum value, limiting the achievable inverter output voltage and reducing the ability to accurately track current references, thereby degrading fault ride-through performance.

B. Saturation Effect of PI Controller on dq-Components

The control law for a PI controller is:

$$u(t) = K_p e(t) + K_i \int_0^t e(\tau)\, d\tau, \quad (5)$$

where $e(t) = i_{\mathrm{ref},d}(t) - i_d(t)$ is the tracking error. If the control output saturates, the integral term continues to grow, causing *integrator windup* and reducing the controller's effectiveness. When $u_{\mathrm{sat}}(t) = u_{\max}$ in (4), the error $e(t)$ persists, leading to:

$$\int_0^t e(\tau)\, d\tau \to \infty \quad \text{if } u(t) \text{ stays saturated.}$$

As a result, the dq-currents $i_d(t)$ and $i_q(t)$ lag their reference values, reducing current-tracking accuracy and slowing the inverter's dynamic response, thereby prolonging the transient period.

C. PWM Saturation Effects on dq-Components During Faults

In addition to PI current controller saturation, other components of the inverter's control system, such as the PWM unit, may also experience saturation. These saturations occur when the control system reaches its operational limits, constraining the inverter's ability to modulate terminal voltage to accurately track the reference signals.

1) Modified dq-Dynamics with Saturation: During PWM saturation, the voltages $v_d(t)$ and $v_q(t)$ are clamped to their respective maximum values. Although the grid voltages $v_{\mathrm{g},d}(t)$ and $v_{\mathrm{g},q}(t)$ can undergo rapid changes during faults, it is reasonable to assume these voltages remain constant during the brief saturation period for the sake of simplifying the subsequent analysis. Under these assumptions, the control signals are limited as:

$$\mathrm{sat}(v_d(t) - v_{\mathrm{g},d}(t)) = u_{\max,d}, \quad \mathrm{sat}(v_q(t) - v_{\mathrm{g},q}(t)) = u_{\max,q}.$$

The dynamic equations become:

$$\frac{di_d(t)}{dt} = -\frac{R_f}{L_f} i_d(t) + \omega i_q(t) + \frac{u_{\max,d}}{L_f}, \quad (6)$$

$$\frac{di_q(t)}{dt} = -\frac{R_f}{L_f} i_q(t) - \omega i_d(t) + \frac{u_{\max,q}}{L_f}. \quad (7)$$

These coupled equations illustrate how both the d- and q-axis currents are influenced by the interaction between active and reactive components, as well as by the limited control signals.

2) Solution for dq-Currents Under Saturation: The solution to the coupled system reflects both the transient and steady-state behavior. For the d-axis current $i_d(t)$:

$$i_d(t) = e^{-\frac{R_f}{2L_f}t} \left(C_1 \cos(\omega t) + C_2 \sin(\omega t)\right) + \frac{u_{\max,d} + \omega L_f u_{\max,q}}{R_f + \omega^2 L_f^2}. \quad (8)$$

979-8-3315-8138-1

Similarly, the solution for the q-axis current $i_q(t)$ is:

$$i_q(t) = e^{-\frac{R_f}{2L_f}t}\left(C_3\cos(\omega t) + C_4\sin(\omega t)\right) - \frac{\omega L_f(u_{\max,d}+\omega L_f u_{\max,q})}{R_f+\omega^2 L_f^2}. \quad (9)$$

where C_1 and C_2 are constants determined by initial conditions. These solutions highlight key characteristics of the dq-currents during saturation:

- **Exponential Decay**: The transient response of the currents decays with a time constant $\tau = \frac{2L_f}{R_f}$, reflecting the impact of the filter parameters.
- **Oscillatory Components**: The cosine and sine terms represent oscillations at the grid frequency ω, indicating the interplay between the d- and q-axis currents.
- **Steady-State Values**: The steady-state currents depend on the saturation limits $u_{\max,d}$ and $u_{\max,q}$. If these limits are too restrictive, the inverter may fail to inject sufficient current during faults.

3) Phase Shift Dynamics: Due to the coupling between the d- and q-axis currents, phase shifts emerge in the transient response. The general form of the oscillatory solutions from (8) and (9) is:

$$i_d(t) \propto \cos(\omega t + \phi_d), \quad i_q(t) \propto \sin(\omega t + \phi_q), \quad (10)$$

where ϕ_d and ϕ_q are phase offsets. The phase difference between the two currents is: $\Delta\phi = \phi_q - \phi_d$. This phase shift arises because the saturated control inputs limit the ability of the inverter to track the reference currents perfectly, leading to a delay between active and reactive power responses.

4) Impact on Fault Response: Saturation degrades the inverter's fault response by inducing oscillatory interactions between the d- and q-axis currents at the grid frequency ω, prolonging transient recovery due to capped control inputs, and reducing active and reactive power injection through phase misalignment between the inverter current and grid voltage.

D. Insufficient Fault Current Injection

To protect internal components, the inverter enforces a current limit during abnormal grid conditions, which can be modeled as

$$|I(t)| = \min\left(I_{\text{ref}}, I_{\text{lim}}\right). \quad (11)$$

When the reference current exceeds the allowable limit, i.e., $I_{\text{ref}} > I_{\text{lim}}$, the inverter injects a maximum current of I_{lim}. As a result, the fault current contribution is constrained, limiting the inverter's ability to support grid voltage during faults.

E. Oscillations Due to Nonlinear Dynamics

When the inverter operates near its limits—such as during controller saturation or current limiting—it exhibits nonlinear behavior. These nonlinearities can cause oscillations in the dq-currents, which impact the inverter's stability and performance.

1) Coupled dq-Currents and Perturbed Dynamics: The dynamics of the dq-currents are given by (6) and (7). These equations describe the interaction between the d-axis and q-axis currents, where the coupling terms $\omega L_f i_q(t)$ and $-\omega L_f i_d(t)$ create cross-dependencies between the two currents. This coupling leads to oscillations, especially when the system operates near saturation or with current limiting.

2) Linearization Around Steady-State: To analyze the oscillatory behavior, we linearize the equations around the nominal operating point:

$$i_d(t) = i_d^0 + \Delta i_d(t), \quad i_q(t) = i_q^0 + \Delta i_q(t), \quad (12)$$

where i_d^0 and i_q^0 are the nominal steady-state values, and $\Delta i_d(t)$ and $\Delta i_q(t)$ represent small deviations from the steady-state. Substituting into the original equations and neglecting higher-order terms, we obtain the perturbed linearized equations:

$$\frac{d\Delta i_d(t)}{dt} = -\frac{R_f}{L_f}\Delta i_d(t) + \omega\Delta i_q(t), \quad (13)$$

$$\frac{d\Delta i_q(t)}{dt} = -\frac{R_f}{L_f}\Delta i_q(t) - \omega\Delta i_d(t). \quad (14)$$

3) Solution of the Linearized System: Taking the time derivative of the first equation and substituting into the second equation, we obtain a second-order differential equation for $\Delta i_d(t)$:

$$\frac{d^2\Delta i_d(t)}{dt^2} + \frac{R_f}{L_f}\frac{d\Delta i_d(t)}{dt} + \omega^2\Delta i_d(t) = 0. \quad (15)$$

This is a standard second-order differential equation, whose general solution is:

$$\Delta i_d(t) = Ae^{-\frac{R_f}{2L_f}t}\cos\left(\sqrt{\omega^2 - \left(\frac{R_f}{2L_f}\right)^2}\,t + \phi\right), \quad (16)$$

where A is the amplitude of the oscillation, ϕ is the phase shift of the oscillation, and $\omega_{\text{osc}} = \sqrt{\omega^2 - \left(\frac{R_f}{2L_f}\right)^2}$ is the damped frequency of oscillation.

4) Conditions for Oscillations: For oscillations to occur, the following conditions must be satisfied:

- $\omega^2 > \left(\frac{R_f}{2L_f}\right)^2$: The grid frequency must be large enough compared to the system's natural damping.
- $u_{\text{sat}} \neq 0$: The control signal must be in a saturated state or switch between saturated and unsaturated regions.

If the system repeatedly switches between saturated and unsaturated states, *limit-cycle oscillations* can occur, where the currents oscillate with a constant amplitude.

5) Impact of Oscillations on Inverter Performance: Oscillations arising from nonlinear dynamics degrade inverter performance by reducing stability, increasing harmonic distortion, and prolonging transient recovery following grid disturbances.

IV. Impact of PLL Errors on dq-Components

During faults or unbalanced conditions, the PLL introduces errors in the estimated angle and frequency, which affect the dq-transformation and the inverter's performance.

A. Mathematical Representation of PLL Errors

The estimated grid angle from the PLL is denoted as $\hat{\theta}_{\text{PLL}}(t)$. If the PLL tracking is imperfect, the estimated angle

979-8-3315-8138-1

deviates from the actual grid angle $\theta(t)$, introducing an *angle error*:

$$\Delta\theta(t) = \hat{\theta}_{\text{PLL}}(t) - \theta(t). \tag{17}$$

Similarly, the estimated frequency $\hat{\omega}_{\text{PLL}}(t)$ may differ from the actual frequency $\omega(t)$, leading to a *frequency error*:

$$\Delta\omega(t) = \hat{\omega}_{\text{PLL}}(t) - \omega(t). \tag{18}$$

B. Impact of Angle Errors on dq-Components

In the ideal case, the dq-components are related to the abc currents as:

$$\begin{bmatrix} i_d(t) \\ i_q(t) \end{bmatrix} = \frac{2}{3}\begin{bmatrix} \cos\theta(t) & \cos\left(\theta(t) - \frac{2\pi}{3}\right) & \cos\left(\theta(t) + \frac{2\pi}{3}\right) \\ \sin\theta(t) & \sin\left(\theta(t) - \frac{2\pi}{3}\right) & \sin\left(\theta(t) + \frac{2\pi}{3}\right) \end{bmatrix} \begin{bmatrix} i_a(t) \\ i_b(t) \\ i_c(t) \end{bmatrix}. \tag{19}$$

However, with an angle error $\Delta\theta(t)$, the transformed dq-currents are given by:

$$i_d^{\text{err}}(t) = i_d(t)\cos(\Delta\theta(t)) + i_q(t)\sin(\Delta\theta(t)), \tag{20}$$

$$i_q^{\text{err}}(t) = -i_d(t)\sin(\Delta\theta(t)) + i_q(t)\cos(\Delta\theta(t)). \tag{21}$$

1) Active-Reactive Power Coupling Due to Angle Error: In the ideal case (with no angle error), the active power $P(t)$ and reactive power $Q(t)$ are decoupled:

$$P(t) = v_d(t)i_d(t), \quad Q(t) = v_q(t)i_q(t). \tag{22}$$

However, with angle error $\Delta\theta(t)$, the currents are misaligned, and leakage occurs between the d- and q-axis components. The new active and reactive powers become:

$$P^{\text{err}}(t) = v_d(t)\left[i_d(t)\cos(\Delta\theta(t)) + i_q(t)\sin(\Delta\theta(t))\right], \tag{23}$$

$$Q^{\text{err}}(t) = v_q(t)\left[-i_d(t)\sin(\Delta\theta(t)) + i_q(t)\cos(\Delta\theta(t))\right]. \tag{24}$$

The angle error $\Delta\theta(t)$ introduces unwanted coupling between active and reactive power, degrading the inverter's power control during faults and unbalanced conditions.

2) Impact on Fault Response:: Angle estimation errors introduce active–reactive power coupling due to cross-leakage between reference frames and delay current recovery during transients as a result of frame misalignment.

C. Impact of Frequency Errors on dq-Components

When the PLL introduces a frequency error $\Delta\omega(t)$, the dq-reference frame rotates at an incorrect speed, causing oscillations in the dq-currents. The modified dynamic equations are:

$$\frac{di_d(t)}{dt} = -\frac{R_f}{L_f}i_d(t) + (\omega + \Delta\omega(t))\,i_q(t) + \frac{v_d(t) - v_{\text{inv},d}(t)}{L_f}, \tag{25}$$

$$\frac{di_q(t)}{dt} = -\frac{R_f}{L_f}i_q(t) - (\omega + \Delta\omega(t))\,i_d(t) + \frac{v_q(t)}{L_f}. \tag{26}$$

1) Oscillations Due to Frequency Error: To understand the impact of frequency errors, we take the second derivative of the d-axis current equation:

$$\frac{d^2 i_d(t)}{dt^2} + \frac{R_f}{L_f}\frac{di_d(t)}{dt} + (\omega + \Delta\omega(t))^2\, i_d(t) = 0. \tag{27}$$

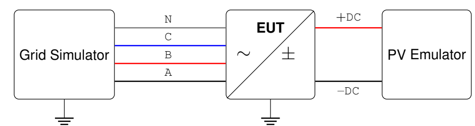

Fig. 2. Experimental setup showing the connection between the Grid Simulator, EUT, and PV Emulator.

This is a second-order differential equation, whose solution is:

$$i_d(t) = A_{\Delta\omega}\, e^{-\frac{R_f}{2L_f}t} \cos((\omega + \Delta\omega(t))\, t + \phi_{\Delta\omega}), \tag{28}$$

where $A_{\Delta\omega}$ and $\phi_{\Delta\omega}$ denote the oscillation amplitude and phase shift under PLL frequency error. The frequency error $\Delta\omega(t)$ shifts the effective oscillation frequency of the dq-currents, thereby reducing control effectiveness during faults.

2) Impact on Fault Response: Frequency estimation errors induce oscillations in the dq-currents, reducing control effectiveness, and amplify negative-sequence oscillations, complicating fault detection and protection.

V. Experimental Validation

A commercial off-the-shelf (COTS) grid-following inverter was tested using the experimental setup shown in Fig. 2 to validate the analytical dq-current dynamics and nonlinear fault-response mechanisms developed in this paper. Balanced and unbalanced faults were applied at $t = 0.2$ s using a programmable grid simulator, and inverter voltages and currents were measured at the point of common coupling.

Fig. 3 shows the measured dq-currents and phase voltages during a balanced fault with a positive-sequence voltage of 0.803 pu, where i_d and i_q exhibit a transient oscillatory response that decays as the system reaches a new steady state. This behavior is consistent with the analytical solutions in (8)–(9), which predict exponentially damped dq-current oscillations arising from dq-axis coupling under saturation. In contrast, Fig. 4 illustrates the inverter response to an LG fault with a comparable positive-sequence voltage of 0.8163 pu, where the dq-currents—particularly i_q—exhibit persistent oscillations that do not fully decay in steady state. This sustained behavior directly supports the theoretical analysis of asymmetrical faults, where negative-sequence components, control saturation, and PLL-induced angle and frequency errors introduce continuous dq-axis coupling as described by (6)–(7) and the PLL-perturbed dynamics in Sections III–IV.

To further examine the fault response, a harmonic analysis of the dq-currents was performed over two intervals: the transient period immediately following fault inception ($0.2 \leq t < 0.3$ s), and the fault steady-state period ($t \geq 0.3$ s).

979-8-3315-8138-1

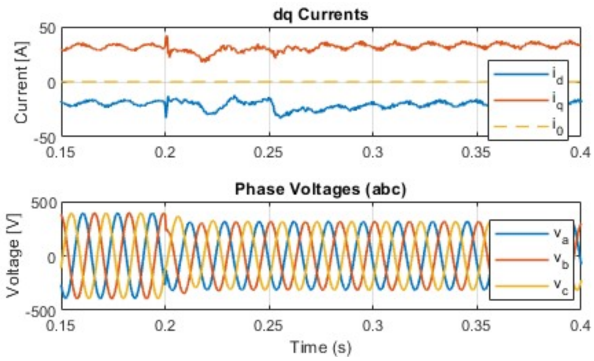

Fig. 3. Measured dq-currents and phase voltages during a balanced fault.

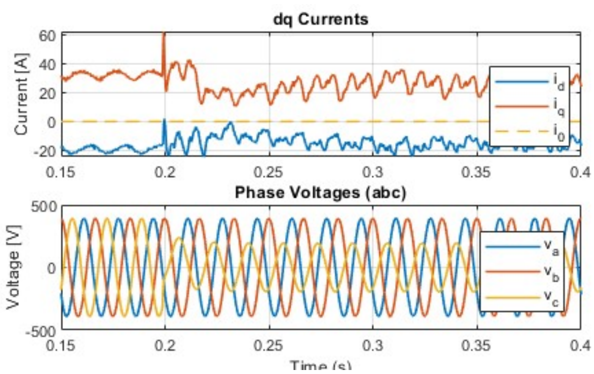

Fig. 4. Measured dq-currents and phase voltages during a LG fault.

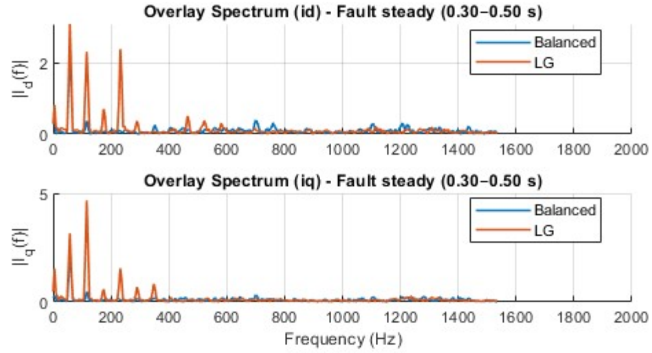

Fig. 5. Frequency-domain representation of dq-currents during the fault steady-state interval.

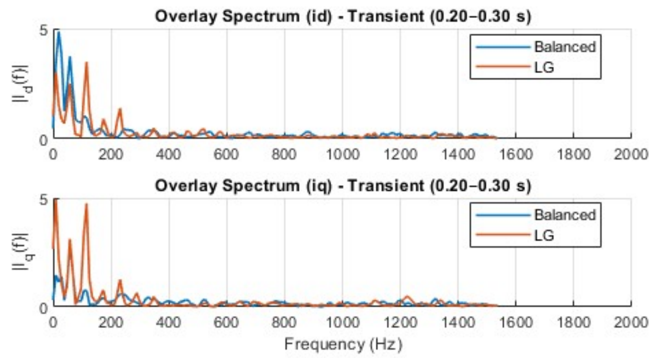

Fig. 6. Frequency-domain representation of dq-currents during the fault transient interval.

As shown in Fig. 5, the balanced fault case exhibits low-frequency oscillations and harmonic components near the grid frequency during the transient interval, which decay as the system reaches steady state, consistent with analytically predicted saturation-induced dynamics dominated by filter damping. In contrast, the LG fault response illustrated in Fig. 6 shows pronounced low-frequency components (on the order of a few hertz) and strong even-order harmonics, including double-frequency components near 120 Hz, that persist into the fault steady-state interval. These sustained spectral features directly support the analytical predictions of nonlinear dq-current dynamics and PLL-induced coupling, which indicate degraded dq decoupling and limit-cycle–like oscillations under asymmetrical fault conditions.

VI. Conclusion

This study provides a comprehensive analysis of IBRs under grid disturbances, focusing on the dynamics of dq-currents. Through a mathematical framework, we captured the behavior of dq-currents during both normal operation and faults, highlighting the role of non-linearities such as controller saturation and current limiting. The derived solutions demonstrate how these non-linearities introduce oscillations, phase shifts, and delays in the transient response, complicating fault ride-through performance and grid stability. Experimental validation with a commercial inverter subjected to balanced and unbalanced faults supports the theoretical predictions. Observations revealed transient spikes, active-reactive coupling, and prolonged settling times, which align with the impact of time constants and saturation effects derived from the mathematical analysis.

References

[1] R. Mahmud, D. Narang, and A. Hoke, “Reduced-order parameterized short-circuit current model of inverter-interfaced distributed generators,” *IEEE Transactions on Power Delivery*, vol. 36, no. 6, pp. 3671–3680, 2021.

[2] R. Mahmud, A. Hoke, and D. Narang, “Fault response of distributed energy resources considering the requirements of IEEE 1547-2018,” in *2020 IEEE Power /& Energy Society General Meeting (PESGM)*, 2020, pp. 1–5.

[3] *IEEE Standard for Interconnection and Interoperability of Inverter-Based Resources Interconnecting with Associated Transmission Electric Power Systems*, IEEE Std. IEEE Std 2800-2022, 2022.

[4] ENTSO-E, “Network code on requirements for generators,” Commission Regulation (EU) 2016/631, 2016. [Online]. Available: https://www.entsoe.eu

[5] National Grid ESO, “GC0111: Fast fault current injection specification,” Grid Code Modification Proposal, 2018. [Online]. Available: https://www.nationalgrideso.com

[6] R. Mahmud, O. Cornmesser, S. Chakraborty, J. Wang, A. Hoke, J. Cale, B. K. Johnson, P. Pinheiro, and R. G. Bainy, “A parametric reduced-order model for inverter short-circuit response in protection studies,” in *Proceedings of the IEEE PES Transmission and Distribution Conference and Exposition (T&D)*, 2026.

979-8-3315-8138-1